Available at: http://publications.ictp.it IC/2008/056

United Nations Educational, Scientific and Cultural Organization
and
International Atomic Energy Agency

THE ABDUS SALAM INTERNATIONAL CENTRE FOR THEORETICAL PHYSICS

POSITRON PROBING OF ELECTRON MOMENTUM DENSITY IN GaAs-AlAs SUPERLATTICES AND RELATED MATERIALS

N.Yu. Arutyunov*
Arifov Institute of Electronics, Tashkent 700187, Uzbekistan
and
The Abdus Salam International Centre for Theoretical Physics, Trieste, Italy

and

N. Sekkal
Departement de Physique-Chimie, Ecole Normale Supérieure de l'Enseignement Technique, BP 1523, El M'Naouer, 31000 Oran, Algeria,
Physia-Laboratory, BP 47 (RP), 22000 Sidi Bel Abbès, Algeria
and
The Abdus Salam International Centre for Theoretical Physics, Trieste, Italy.

MIRAMARE – TRIESTE

August 2008

* Corresponding author: n_arutyunov@yahoo.com

Abstract

The band structure calculations based on the method proposed by Jaros et al. (*Phys. Rev. B 31, 1205 (1985)*) have been performed for the defect-free GaAs-AlAs superlattice and related AlAs and GaAs single crystals; the electron-positron momentum density distributions have been computed and analyzed.

The results of calculations are in good agreement with the experimental data obtained *ad hoc* for GaAs and AlAs bulk materials by measuring the angular correlation of the annihilation radiation (ACAR). Small (but marked) features of the electron-positron momentum density of the valence band have been revealed both for constituent materials and GaAs-AlAs superlattice.

The delocalization of positron in "perfect" defect-"free" AlAs and GaAs single crystals to be observed experimentally is borne out by the results of pseudo-potential band calculations performed on the basis of method proposed by Sekkal et al. (*Superlattices and Microstructures, 33, 63 (2003)*). The prediction of the possibility of a certain confinement of positron in the interstitial area of GaAs-AlAs superlattice is confirmed by the agreement between the results of calculations and relevant experimental data obtained for GaAs and AlAs single crystals. No considerable effect of the enhancement of the annihilation rate (due to electron-positron interaction) upon the electron-positron momentum density distribution both in the superlattice and its constituent bulk materials has been found.

The results of ACAR measurements and calculations performed suggest that a tangible improvement of the sensitivity of existing positron annihilation techniques is necessary for studying details of the electron-positron momentum density distributions in defect-"free" superlattices to be created on the basis of the diamond-like semiconductors possessing close values of the electron momentum densities. On the contrary, the positron-sensitive vacancy-type defects of various types in the superlattice may become a source of the annihilation radiation whose momentum density distribution has its own peculiarities, different from the ones to be detected for defect-"free" crystal structure. Being a "fingerprint" of a certain type of defects these peculiarities make it possible the non-destructive characterization of the heterostructures and superlattices by means of the positron particle microprobe.

1. Introduction

An increasingly intensive use of the heterostructures in the semiconductor technology puts forward a problem of studying the microstructure of vacancy-type defects in them. Almost the only method of obtaining such data is the positron probing both the free volume and ion cores of its environment in the crystal lattice (see e.g. [1] and references therein). As various superlattices and quantum wells are being created now on high-quality GaAs substrates, the lattice-matched GaAs-AlAs heterostructure is especially attractive for the positron diagnostics of defects in it.

However, here we will have to face a challenge of detecting annihilation radiation which might serve as a fingerprint of a certain defect. The matter is that GaAs-AlAs superlattices are created in the form of rather thin layers for which they might have been reliably probed with the slow positron beams available at present. The other complication is that the electron densities of the constituent binary zinc-blend structures possess close electron-momentum density distributions to be characterized by the magnitudes of the averaged electron densities $r_s \approx 2{,}081\ a.u.$ and $r_s \approx 2{,}11\ a.u.$ for GaAs and AlAs, respectively (we will discuss this question below; see, e.g. Sec.5). The difference between these numeral values does not exceed ~ 1.5% that creates additional both theoretical and experimental difficulties in studying GaAs-AlAs superlattice by the methods of positron spectroscopy.

The most sensitive way of studying such a small difference of the electron density and its momentum distribution is based on both calculations and measurements of the angular correlation of the annihilation radiation (ACAR), and so we attempted to carry out the investigation of the electron-positron momentum distribution both in GaAs-AlAs superlattice and its constituents using this particular method.

The results obtained suggest that one can create a reliable procedure for non-destructive/non-contact characterization of GaAs-AlAs superlattice as well as point vacancy-type defects in it. In this connection the positron confinement in ideal perfect defect-"free" superlattice must be studied from the point of view of its influence on a possible transition of positron into the trapped state at a vacancy-type defect.

It is well known that the methods of positron annihilation spectroscopy are most effective when we have an opportunity of suitable comparative investigation. Recently, three-dimensional confinement of positron in defect-"free" Cu precipitates formed by the thermal aging in diluted Fe-Cu alloys has been observed [2]. Its existence in the alloys under consideration has been proved by means of comparing the positron lifetime with the one obtained on the basis of *ab initio* calculations performed for the bulk of Cu metal.

In this connection one should mention the rather successful research on the positron probing of α-Si and SiO_2 materials deposited on p-Si [100] substrate with the purpose of creating a superlattice-like structure [3]: in this work the parameters of the Doppler broadening of the annihilation radiation spectroscopy (DBAR) have been determined for the interface between the layer and the substrate in order to analyze them, having used the relevant data obtained for the bulk of both α-Si and SiO_2 materials.

The problem of a confinement of positron in the quantum well superlattices has been studied theoretically in [4]. It has been predicted that depending on both energetic and configuration parameters of the superlattice positrons can be confined in specific regions just like the electrons and, for the lack of a better term, the term "positron superlattice" has been used. It should be emphasized that the abovementioned prediction concerning the confinement of positron has been made for the defect-"free" semiconductor heterostructures, thus confirming qualitatively the abovementioned data available for diluted Fe-Cu alloys [2].

The trapping as well as a confinement or a partial localization of positron in a certain region of the superlattice, - all these states mean implicitly that positron will annihilate there and two gamma-quanta to be emitted out of the sample will bear direct elemental specific information concerning both the electron density and the ion core environment around the positron in a certain nano- or sub-nano-sized region of the sample [1]. A crucial point, however, is that one must separate the flow of annihilation radiation, related to the "perfect" crystal, from the one resulted from the positron trapping by defects.

The results of systematic pseudopotential calculations in GaAs-AlAs superlattice are described in this paper. Inasmuch as the positron diagnostics has not been applied yet for studying the electron-positron momentum density distribution in GaAs-AlAs heterostructures, we have tried estimating merits and demerits of this method on the basis of data obtained by high-precision spectroscopy of the angular correlation of the annihilation radiation (ACAR) for relevant bulk materials, GaAs and AlAs. Then we have compared the data available with the results of computations performed for both GaAs-AlAs superlattice and its abovementioned constituents.

The results of the comparative analysis of the data obtained suggest a certain partial confining of the thermalized positron in the free volume of GaAs-AlAs superlattice. This confinement of positron is supposed to change to the positron trapping by the vacancy-type defects formed in the sub-lattices of the superlattice: in passing from the confinement regime to the trapped state considerable changes of the electron-positron momentum distribution of the annihilation radiation are observed. Being processed as a "fingerprint" of the microstructure of a certain point defects, such electron-positron momentum distributions may find practical applications for non-destructive characterization of the semiconductor superlattices (e.g., for the positron diagnostics of the vacancy-type damages in the GaAs component part of the heterostructures GaAs-AlAs, see below).

2. Experimental

The long-slit scheme of the installation possessing the angular resolution ~ 0,9 mrad (1 milliradian = $10^{-3}\, m_0 c \approx 0.137$ *a.u.* $\approx 0{,}057°$) has been used for measuring the ACAR spectra at room temperature (for more details see [5] and references therein). Thus, the precision of studies of the electron-positron momentum densities was, approximately, higher by a factor of ~ 5 than the one of measuring the Doppler broading of the annihilation radiation (DBAR)[1].

[1] This circumstance, - namely, the angular resolution of the ACAR measurements, - turned out to be crucial for correct comparing very close electron-positron momentum densities of the valence bands which are characteristic of AlAs and GaAs diamond-like semiconductors (see below, Sec. 4 and Fig.6 for more detail).

We shall give only a short account of the samples of GaAs material which has been selected *ad hoc* and whose parameters will be considered elsewhere in more detail. Single crystal *n*-GaAs<Si>, n~10^{17} cm^{-3}, oriented along [111], [100], and [110] crystallographic direction, were subjected to special treatment including the annealing of the sample in order to minimize the concentration of possible vacancy-type defects including $EL2$ arsenic antisites. On the contrary, as-grown material containing vacancy-type point defects was used for demonstrating their role in forming those electron-positron momentum distributions which are related to the positron trapping by defects.

The samples of AlAs were oriented along [111], [110] and [100] crystallographic directions in the process of recording of ACAR spectra, and special precautionary anti-corrosion measures were undertaken. The details of ACAR studies of AlAs binary compound as well as its thick layers (thickness > 80 microns) grown by long-term molecular beam epitaxy on GaAs substrates will be discussed elsewhere.

These samples of AlAs and GaAs single crystals were used for determining the difference between both ACAR spectra and corresponding electron-positron momentum density distributions; then the comparison of experimental and calculated data has been performed.

3. Calculations of partial and total electron-positron momentum density distributions in GaAs-AlAs superlattice

3.1. Framework of calculations

We have used the empirical pseudopotential method (EPM) for obtaining parameters of the electron states in the band structure that enable studying large cells relevant to the task to be considered in this particular paper; this method is known to omit determining properties of the electron core states [6].[2] The eigenvalue equations are given in the following form:

$$\left[\frac{\hbar^2}{2m_e}\left(\vec{K}_b+\vec{G}_n\right)^2-E\right]A_{n\vec{k}}+\sum_m S\left(\vec{G}_m-\vec{G}_n\right)V\left(\vec{G}_m-\vec{G}_n\right)A_{m\vec{k}}=0\ . \tag{1}$$

Here, for simplicity, the spin-orbit interaction is not taken into account; $A_{n\vec{k}}$ is a complex constant, $\vec{K}_b$ is the wave vector, m_e is the free electron mass, $\hbar = h/2\pi$ is the Planck's constant, and, at last, $\vec{G}_m$ and $\vec{G}_n$ are the reciprocal lattice vectors (for more details see [6]). V($\vec{G}_m$ - $\vec{G}_n$) and S($\vec{G}_m$ - $\vec{G}_n$), are the form factor and the structural factor, respectively. Hence, the sum

$$\xi_{\vec{K}b}\left(\vec{r}\right)=const\sum_{\vec{G}}A_{n\vec{K}}\exp\left[i\left(\vec{K}_b+\vec{G}\right)\vec{r}\right] \tag{2}$$

represents the wave functions of the electron states of the bulk material.

Once the parameters of the electron structure are obtained one may determine the positron states. The independent particle model (IPM) has been applied for calculating the positron band

[2] Starting from the data available on the probability of the positron penetration into the core region in solids we have good reason to believe that this simplification is quite justifiable for the materials under study [1].

structure (for more details see, e.g. [7]). This method is rather accurate for GaAs and AlAs semiconductors in which the enhancement of the positron annihilation rate is known to be relatively small (see also below, Sec.4 for more details). Though the IPM approximation does not take into account the electron-positron interaction, nevertheless, this approach is justifiable for the electron Fermi gas of a relatively high density (n) whose magnitude is equal to $r_s = (3/4\pi\, n)^{1/3} \approx 2\ a.u.$[3]

Indeed, the local density approximation (LDA), which takes into account the screening electron cloud around the positron, as well as generalized gradient approximation (GGA) connecting IPM and LDA, - these three ways of calculations are known to result in close electron-positron momentum distributions for a majority of solids (and even, in particular, for organic conductor TTF-TCNQ [10])[4]. Bearing in mind these remarks we will find the positron wave function in the form similar to the one found for electrons (see Eq. (2)); here again, just as it has been done for the electron states, one must solve the following system of equations:

$$\left[\frac{\hbar^2}{2m_p}\left(\vec{K}_b + \vec{G}_n\right)^2 - E\right]B_{n\vec{k}} + \sum_m W\left(\vec{G}_m - \vec{G}_n\right)B_{m\vec{k}} = 0\,, \tag{3}$$

where the sum contains the Fourier transforms of the Coulomb potential and the total charge density of bonding electrons, $\rho^{\,n}\left(\vec{G}_m - \vec{G}_n\right)$and $\rho^{\,e}\left(\vec{G}_m - \vec{G}_n\right)$, respectively:

$$W\left(\vec{G}_m - \vec{G}_n\right) = \frac{8\pi}{\left|\vec{G}_m - \vec{G}_n\right|^2}\left(\rho^{\,n}\left(\vec{G}_m - \vec{G}_n\right) + \rho^{\,e}\left(\vec{G}_m - \vec{G}_n\right)\right); \tag{4}$$

$$\rho^{\,n}\left(\vec{G}_m - \vec{G}_n\right) = \frac{Z_V}{\Omega}\ ; \tag{5}$$

$$\rho^{\,e}\left(\vec{G}_m - \vec{G}_n\right) = \frac{1}{\Omega}\int d\vec{r}\,\rho^{\,e}\left(\vec{r}\right)\exp\left[-i\left(\vec{G}_m - \vec{G}_n\right)\vec{r}\right]. \tag{6}$$

Total charge density $\rho^{\,e}\left(\vec{r}\right)$ can now be calculated from the electron wave functions satisfying Eq. (2); here $B_{n\vec{k}}$ is a complex constant, m_p is the free electron mass in Eq. (3). The number of bonding electrons Z_v depends on the chemical nature of atom and Ω designates the volume of integration in Eq. (6). The positron wave functions are calculated by means of the equation similar to Eq. (2):

$$\Psi_{\vec{K}\,b}\left(\vec{r}\right) = const\sum_{\vec{G}} B_{n\,\vec{K}}\,\exp\left[i\left(\vec{K}_b + \vec{G}\right)\vec{r}\right]. \tag{7}$$

---

[3] This is not the case for relatively low electron densities to be characterized by r_s magnitudes over the range ~ 4 ÷ 6 a.u. (which are characteristic of, e.g., the alkali metals; for more details see, e.g. [8, 9]).

[4] For diamond-like semiconductors the magnitudes of r_s calculated by IPM, LDA and GGA are close to each other, too, though the calculations based on IPM result in small (but marked) deviations from the data obtained by GGA [9].

Now, once the bulk eigensystems of both electrons and positrons have been determined, we can go over to calculating both electron and positron charge and momentum distributions for the $(GaAs)_m$-$(AlAs)_n$ superlattice, respectively (m and n are the number of monolayers of GaAs and AlAs). A monolayer consists of two monoatomic planes composed by the cation and the anion atoms, respectively.

We have used the method proposed by Jaros et al. [11] in which the calculation of the electron charge and momentum distribution in GaAs-AlAs superlattice is carried out in succession. First, we calculate the eigensystem belonging to the one of the two bulk materials constituting the superlattice, namely (for certainty), to the bulk GaAs single crystal and, secondly, the atoms of GaAs are replaced by the atoms of GaAs-AlAs superlattice at the relevant sites (the procedure of such replacement has already been described in [11,12]); for the lack of a better term, the single crystal of GaAs is called a "host bulk material". It also means that the wave function for the superlattice is to be written as a linear combination of the wave functions corresponding to the single crystal of GaAs. So long as the electron density distributions of bonding electrons in GaAs and AlAs diamond-like semiconductors are known to be close to each other, we have to emphasize the fact that the choice of concrete host bulk material either GaAs or AlAs does not exert a marked influence on the final results of calculations.

A common way of obtaining the states for both electron and positron in the superlattice is the one in which for a given wave vector $\vec{k}_{SL}$ of the superlattice one can write the wave function $\Phi_{\vec{K}\,sl}$ as a linear combination of the bulk wave functions; $\Psi_{\vec{k}_B}$, $\vec{k}_B$ are the set of the bulk wave vectors which are equivalent to $\vec{k}_{SL}$ vector. This set is unambiguously calculated by the formula $\vec{K}_B = \vec{K}_{sl} \pm \frac{2\pi}{a}\left(\frac{1}{m+n},0,0\right)$ which is justifiable for the directions of high symmetry (which are considered in this work). Therefore, we can determine the wave function as a linear combination:

$$\Phi_{\vec{K}\,sl} = const \sum_n \sum_{\vec{K}_b} C_{n\vec{K}\,b} \Psi_{n\vec{K}\,b}(\vec{r}) \,. \tag{8}$$

When obtaining eigenvalues of this function one should solve the following equation:

$$(H_0 + \Delta V)\Phi_{\vec{K}\,sl} = E_{sl}\Phi_{\vec{K}\,sl} \,, \tag{9}$$

where H_0 is the unperturbed Hamiltonian corresponding to GaAs constituent material (see above for more detail), ΔV is the difference between the potential of the atoms in superlattice and the atoms in the bulk material, respectively (this difference is assumed to appear as a result of the replacement of the latter ones by the former ones). Having substituted the function (8) into Eq. (9) and having multiplied the result by the $\Psi^*_{\vec{k}_B}$ function (i.e., by the complex conjugate of $\Psi_{\vec{k}_B}$ function), one obtains the following secular equation:

$$C_{n'\vec{K}'_b}\left(E_{n\vec{K}b}-E_{sl}\right)+const\sum_{n}\sum_{\vec{K}_b}C_{n\vec{K}b}\int\Psi^{*}{}_{n\vec{K}b}(\vec{r})\;\;\Delta V(\vec{r})\;\;\Psi_{n\vec{K}b}(\vec{r})d\vec{r}=0\,, \tag{10}$$

where E_{sl} is the eigenenergy in the superlattice and $C_{n\vec{K}b}$ are the complex constants which we have to calculate in order to obtain the wave functions corresponding to the electron states in the superlattice; the integration over the total space should be performed in Eq. (10). Numeral values of the constants $C_{n\vec{K}b}$ are used to determine what kinds of the electron states in the bulk material simulate corresponding states in the superlattice.

The band offset parameter is taken into account in our calculation via the electron form factor for a zero reciprocal lattice vector. The magnitude of this vector is fitted to the numeral value obtained experimentally for the band lineups in the GaAs-AlAs superlattices (for more detail see [4,7] and references therein). And, at last, the momentum density distribution of the annihilation radiation is calculated by the generalized formula:

$$\Gamma_{total,SL\quad or\quad B}(\vec{p})=\sum_{n}\Gamma_{n,SL\quad or\quad B}(\vec{p})\,, \tag{11}$$

where *n* is the index of the electron band, $\vec{\mathrm{k}}$ is the wave vector in the Brillouin zone of the superlattice, and $\vec{p}$ is the momentum of two annihilation photons. The summation in Eq. (11) runs over all occupied electron states. The indexes *SL* and *B* are used for distinguishing between the superlattice and the bulk material, respectively; $\Gamma_{n,SL\quad or\quad B}(\vec{p})$ is the partial momentum density for the n^{th} band:

$$\Gamma_{n,SL\quad or\quad B}(\vec{p})=const\sum_{\vec{k}}\left|\int\exp(-i.\vec{p}.\vec{r})\;\;\left(\Psi_{p,SL\quad or\quad B}(n=1,\vec{k}=\Gamma,\vec{r})\;\;\Psi_{e,SL\quad or\quad B}(n,\vec{k},\vec{r}).d\vec{r}\right)\right|^{2}. \tag{12}$$

Eq.(12) may be verified experimentally so long as the momentum distribution of the annihilation radiation is determined, e.g., by means of ACAR or DBAR spectroscopy; we have compared the results of calculation with the relevant experimental data available (see below, Sec. 4).

3.2. Calculated partial electron-positron momentum density distributions in GaAs-AlAs superlattice

The thermalized positron wave function $\Psi_{p,SL}(n=1,\vec{k}=\Gamma,\vec{r})$ is practically unchangeable in passing from the superlattice to the bulk so long as it is renormalized to the volume of superlattice. Therefore, the positron wave functions are assumed to be the same in the investigated materials: our calculations show that the final results do not vary considerably as a result of this simplification and the renormalization constant disappears after integration.

The electron wave functions $\Psi_{e,SL}(n,\vec{k},\vec{r})$ related to the superlattice are all those ones that correspond to the valence subbands. We would like to remind the reader that their number is equal to $4(\mathrm{m}+\mathrm{n})$, where *m* and *n* are the numbers of GaAs and AlAs monolayers[5], respectively, and each monolayer contains the pairs of the anion and cation atoms; the Brillouin zones (BZ) of both bulk

[5] Or the atomic planes in the other designations (see, e.g. [4]).

GaAs (or AlAs) single crystal and $(GaAs)_u$-$(AlAs)_v$ superlattice are shown in Fig. 1 (the indexes u and v correspond to the number of monolayers in the superlattice); two superlattices having u and v equal to 1 and 2, respectively, are considered below (see also [4] for more details). The high symmetry points of BZ for both the bulk material and the superlattice are shown in Fig. 1 on the right and on the left, respectively.

Obviously, the partial momentum density $\Gamma_{n,SL}(\vec{p})$ of the two-quantum annihilation radiation to be emitted from the superlattice bears information about the partial electron-positron momentum density[6]. These distributions of the electron-positron momentum densities are shown for the four valence bands characterizing the bulk material of GaAs single crystal (see Fig. 2). The partial electron-positron momentum densities calculated for [100] and [011] crystallographic directions for eight and sixteen subbands of $(GaAs)_1$-$(AlAs)_1$ and $(GaAs)_2$-$(AlAs)_2$ superlattices, respectively, are shown in Fig. 3 and Fig. 4. It should be noted that the numeration of subbands in Figs. 2-4 begins from the last valence subband and, thus, it appears in all figures under the number one.

All valence subbands in the bulk of GaAs single crystal have been found to contribute greatly to the annihilation process (Fig. 2). In the case of $(GaAs)_1$-$(AlAs)_1$ superlattice, one can see that five lower subbands have comparable and comparatively large contributions to the process of annihilation, in contrast to the three upper subbands whose contributions to the probability of annihilation are relatively small (see Fig. 4).

The number of valence bands of the $(GaAs)_1$-$(AlAs)_1$ is larger by a factor of two as compared with GaAs bulk material and each pair of two successive superlattice valence bands is supposed to originate from the folding of one valence band of the host bulk material. In turn, each pair of the superlattice valence bands will have to have comparable contribution to the annihilation process. This is, however, not the case when we consider both fifth and sixth subbands whose partial densities of states originates from the third valence band of the bulk material. Qualitatively, the magnitude of the partial density $\Gamma_{5,SL}$ is larger than that of $\Gamma_{6,SL}$ (it is seen visually, e.g., from comparison of the square of the regions occupied by the curves numbers 5 and 6, respectively, in Fig. 3)[7].

So far as we deal with four valence bands in the host bulk material, $(GaAs)_2$-$(AlAs)_2$ superlattice has sixteen valence subbands. In $(GaAs)_2$-$(AlAs)_2$ superlattice all valence subbands have comparable contributions to the partial electron-positron momentum density distributions calculated for [100] and [011] crystallographic directions (see Fig. 4 where the square under each curve is almost one and the same)[8].

---

[6] It will be recalled once again that the electron momentum distribution is practically undistorted by the presence of the positron in the superlattice as the contribution of the thermalized positron into the resulting momentum of the pair of annihilating gamma-quanta is negligibly small; moreover, the positron wave function is assumed to be a constant inasmuch as it varies slowly in passing from the bulk to the superlattice.

[7] A plausible explanation for the difference between the partial densities mentioned above is that the fifth and sixth valence subbands of the superlattice are derived on the basis of different ways of mixing of the valence bands of the GaAs bulk material (this question will be discussed elsewhere in more detail).

[8] Each package of four subbands may be, mostly, derived from the folding of one bulk valence band. The coupling processes are supposed to be small and we do not consider them in this paper.

3.3. Calculated total electron-positron momentum density distribution in GaAs-AlAs superlattice

Of special interest is the total distribution of the electron-positron momentum density in so far as it is this distribution that is detected by ACAR measurements.

In order to calculate such distribution we have superimposed all functions of partial electron-positron momentum densities obtained for $(GaAs)_1$-$(AlAs)_1$ and $(GaAs)_2$-$(AlAs)_2$ superlattices (see Fig.3 and Fig.4). As an example, the result of summation obtained for [011] crystallographic direction is shown in Fig. 5.

It is important to note that *there is observed a saddle-like shape* of the total distribution of the electron-positron momentum density for [011] direction which is characteristic of the momentum density distribution for tetrahedral crystal lattices (see Fig.5)[9]. We would like to draw the reader's attention to two facts of behaviour of the total distribution of the electron-positron momentum density in GaAs-AlAs superlattice: (*i*) the minimum observed at $p_z = 0$ *a.u.* as well as (*ii*) rather abrupt change of the derivative near to the value $p_z \sim 0{,}9$ *a.u.*[10] , - these peculiarities are a fingerprint reflecting the symmetry of the diamond-like crystal lattice. Also, these data indicate *reliability* and correctness of the whole scheme of calculations described above in Sec. 3 inasmuch as these calculated data follow the experimental ones (see below in more detail as well as Fig.6).

In this connection it is important to emphasize observing a step-like drop over the range of momenta from ~ 3,5 to ~ 6×10^{-3} m_0c which, in its turn, is close to the magnitude of the Fermi momentum of the electron-positron momentum density distribution, p_F (see Fig.6). Such behaviour of the electron-positron momentum density distribution is characteristic for [110] crystallographic direction of the elemental diamond-like semiconductors where the step-like drop mentioned above indicates the reflection of waves of the bonding electrons at the Jones zone face (see [1, 13, 14] for more details).

Also, we would like to emphasize that the *behavior of calculated total function of the electron-positron momentum density distribution is similar to the experimental momentum distribution* of the annihilation gamma-quanta obtained for [110] and [100] crystallographic direction in the diamond-like semiconductors (see, e.g. [1] and references therein for more details). It means that positron *is confined in GaAs-AlAs superlattice* inasmuch as As atoms possess the higher affinity for the positron whose partial delocalization on the atoms of anions is observed not only for As atoms in (A^3)As tetrahedral structures but also for all A^3B^5 binary diamond-like semiconductors [1]. The properties of this confinement are predicted to depend on the chemical nature of the layer: probably,

[9] For [100] crystallographic direction of the materials under study there have been obtained similar electron positron momentum distributions possessing of their own anisotropic features; for not to encumber the paper with details we do not present corresponding figures.

[10] Or, using more customary units, p_z is equal to $\approx 6,81 \times 10^{-3}$ m_0c; on the whole, this value is close to the Fermi momentum of the bonding electrons in the single crystals of GaAs and AlAs as well as in GaAs-AlAs superlattice, see Fig. 6. More detailed analysis of relations between these numeral values and the anisotropy of the electron-positron momentum density distributions in GaAs-AlAs superlattice as well as in its constituents will be done elsewhere.

the delocalized positron prefers to be confined in the free volume which provides for more favorable energetic conditions [4].

Last but not least, concerns the total electron-positron momentum density distributions obtained for different crystallographic directions over the range of 0 to ~ 2,5 $\times 10^{-3}$ $m_0 c$ (this interval corresponds to $\Delta p_z \sim 0 \div$ 0,33 *a.u.* in Fig.5; we consider only one symmetrical part for the distribution). In actual fact, a certain mutual compensation of lower and higher contributions of the partial distributions of calculated electron-positron momentum densities always takes place. Total charge, obviously, is conserved, i.e. the function $\Psi_{p,SL}(n=1,\vec{k}=\Gamma_{SL})$ is unchangeable with the accuracy to a constant factor which disappears as a result of integration (see also above, Sec. 3.2). Accordingly, the electron-positron total density of states $\Gamma_{SL,total}(\vec{p})$ in the superlattice is compensated completely by the positively charged ion cores whose total effective charge density is $\rho_{SL.or.Bulk}(\vec{r}) = const.\sum_{occ}\left|\Psi_{SL.or.Bulk}\right|^2$. It means that momenta of the annihilation gamma-quanta bear the information about the charge densities where the positron is, at least, partially (de)localized. With this provision, ACAR measurements can be expected to give acceptable accuracy for finding out differences of the electron-positron momentum densities in the valence bands of GaAs and AlAs single crystals; the experimental data pertinent to this case are compared below with the calculated ACAR distributions obtained for GaAs-AlAs superlattice.

4. Comparison of calculated electron-positron momentum density distribution for GaAs-AlAs superlattice with experimental data for GaAs and AlAs single crystals

When ACAR spectrum is recorded then the probability of detecting a pair of annihilation quanta with a total momentum p is proportional to the average electron-positron momentum:

$$I(p) \cong \iint \Gamma_{total,SL \quad or \quad B}(\vec{p})\, dp_x dp_y \cong const \int_{\theta}^{p_F} p\ \rho(\vec{p})\ dp. \tag{13}$$

where $p \approx \theta \cdot m_0 c \approx p_z$, θ is the angle of detection of a pair of the annihilation quanta, $m_0 c$ is the rest momentum of electron, $I(p)$ is the counting rate of the pairs of the annihilation gamma-quanta, and p_z is the module of the projection of the electron-positron momentum onto a certain axis z which is perpendicular to the axis of rotation of the movable detector of the ACAR spectrometer[11].

In the binary compounds under study, GaAs and AlAs, the function $\rho(p)$, reconstructed from the ACAR spectra, demonstrates the behavior typical for the Fermi distribution near to the Fermi momentum. No components that are usually attributed to the positron localization on defects have been observed for the defect-"free" materials. Moreover, - so long as a conception of delocalized

[11] Actually, the component of the resulting momentum of the pair of gamma-quanta, which is equal to the p_z magnitude of the electron-positron momentum, is detected; they say that the long-slit scheme of the angular spectrometer allows one to record so-called one-dimensional (1D) spectrum of ACAR (for more detail see [1,5] and references therein).

positron has been underlain the calculations both for the constituent materials and GaAs-AlAs superlattice, - a delocalized behaviour of positron is confirmed by a close similarity of reconstructed and calculated $\rho(p)$ distributions.

As it has already repeatedly been mentioned, a thermalized positron makes a relatively small contribution to the total momentum of the annihilating pair, and the parameters of the electron-positron momentum distribution are determined by one component of the pair, i.e. by the electron momentum. Therefore, ACAR spectral function reflects, mostly, the anisotropy of the electron momentum density distribution which depends on the direction in the crystal lattice.

As seen from Fig. 6, the electron-positron momentum density distribution, calculated for GaAs-AlAs superlattice, as well as the one reconstructed for GaAs and AlAs single crystals, - they are very close to each other over the range of a narrow interval of changes of the Fermi momentum of the bonding electrons. Of paramount practical importance is that this interval includes the values of the Fermi momentum calculated by IPM approximation, i.e. for the undisturbed Fermi gas of the valence electrons.[12] It should be emphasized also that the numeral value of calculated Fermi momentum (p_F) follows the changes of FWHM of the electron-positron momentum density distribution in passing from AlAs to GaAs and AlAs-GaAs superlattice, accepting the magnitudes equal to ~ 6.63×10^{-3} m_0c and ~ 6.7×10^{-3} m_0c for AlAs and GaAs, respectively (see Fig.6).

The results obtained clearly show a very close similarity between the electron-positron momentum density distributions in the valence band over the range of momenta close to the Fermi level both in the "host" binary semiconductors (AlAs, GaAs) and their GaAs-AlAs superlattice. So long as this heterostructure is fabricated in the form of the thin film it means that two component layers in the "perfect" structure of the superlattice may be detected reliably provided that both sensitivity and resolution of the positron self-seeking microprobe based on measuring ACAR spectra are tangibly increased. In other words, the solving of the problem of reliability of the positron diagnostics of the superlattices of the diamond semiconductors will inevitably require, at least, a considerable improvement of the brightness of the slow positron beam which is one of the main component parts of the whole procedure of the positron probing of thin and ultrathin layers [13].

But even if this problem had been resolved the electron-positron momentum density distribution would not have been much different from the ones predicted for AlAs-GaAs superlattice (see Fig.6 and Fig.7 as well as experimental data therein). The closeness of the electron-positron momentum density distributions in GaAs and AlAs single crystals imposes a certain natural limitations on the effectiveness of the positron probing of a "perfect" GaAs-AlAs superlattice. It means that, on the other hand, a practical non-contact/non-destructive characterization of GaAs-AlAs

[12] In actual fact, once again we come to the conclusion about a relative insignificance of amendments related to the enhancement factor of the positron annihilation rate in the relatively dense ($r_s \approx 2\ a.u.$) electron Fermi gas, especially, when the matter concerns the electron-positron momentum density distribution; this conclusion is in agreement with the one formulated previously for various materials, in particular, for both diamond-like semiconductors [1] and organic conductors TTF-TCNQ [10]. In turn, it means that one can avoid considerable inaccuracies in the final numeral results when being carried out the calculations of the electron-positron momentum density distributions for the Fermi gases in which the electron-positron interaction is assumed to be inessential.

superlattice would be most effective for non-perfect thin films; we are considering such possibility below.

5. Difference between electron-positron momentum density distributions in the valence band of GaAs and AlAs single crystals

Of paramount importance is a reliable distinguishing of the ACAR spectra which are generated by the sublattices of GaAs-AlAs superlattice inasmuch as the valence band of the both materials is formed by similar sp^3 - hybridized orbitals.

To evaluate qualitively a magnitude of this similarity, we have calculated the difference between the angular correlation of the gamma-quanta to be emitted from the valence zone of AlAs and GaAs single crystals, respectively. As a first step, IPM has been used, within the framework of which the thermalized positron was assumed to annihilate in the ideal non-disturbed Fermi-gas of electrons (see also above, Sec.4, and footnote[12]). Then a disturbed electron density round the positron has been applied for evaluation both the Fermi momentum and the difference between ACAR curves; and, at last, all difference curves obtained by these ways for AlAs and GaAs single crystals have been compared with experimental data.

The calculations of ACAR have been based on some practical schemes in which the enhancement of the electron density at the positron is supposed to depend on the density (n) of the unperturbed electron gas, $r_s = (3/4\pi n)^{1/3}$ [14]. For [111] crystallographic directions the functions of ACAR are closed to the inverted parabola whose crossing of the abscissa at so-called cut-"off " angle is proportional to the Fermi momentum p_F [1]. To this approximation the difference between ACAR functions is determined, mainly, by the magnitudes of the numeral values of the characteristic electron radius $r_s \approx 13{,}99 \times p_F^{-1}$ (r_s and p_F are measured in the atomic units and milliradians, respectively [8, 14]). We have estimated this value using Ferrell's approach in which the numeral value of r_s depends on the ratio of the atomic weight, *A*, to the specific gravity, *d* (g/cm^3) [8]:

$$r_s \cong 1{,}384 \times \sqrt[3]{A/d\,z}\ , a.u., \qquad (14)$$

where z = 4 is the coordination number (or the reduced valence) for the binary A^3B^5 diamond-like semiconductor compounds. As the averaged magnitude of *A* the half of the molecular weight of the A^3-B^5 molecule has been used [1,14][13]. Accordingly, numeral values of r_s are estimated to be equal to $\approx 2{,}11\ a.u.$ and $\approx 2{,}081\, a.u.$ for AlAs and GaAs, respectively (see Fig. 7).

It is interesting to note in this connection that the electron-positron correlation effects, taken into account within both so-called semiconductor and insulator models, *do not influence considerably on the magnitudes of r_s parameter calculated by Eq. (14)*: for AlAs and GaAs there have been

[13] This in itself is a certain approximation, which, however, seems to be quite correct for the calculations of the unperturbed electron densities. Parameter r_s estimated by this way is used to calculate the positron lifetime whose values are in a good agreement with the experimental data available for the diamond-like semiconductors; and, vice versa, r_s values reconstructed by means of the ACAR parameters are very close to the ones estimated by Eq. (14) for unperturbed electron densities for different tetrahedral structures [14].

obtained the numeral values $r_s^{eff} \approx 2{,}35 \div 2{,}4\, a.u.$, and $r_s^{eff} \approx 2{,}439 \div 2{,}375\, a.u.$, respectively [15][14]. Let us estimate how these numeral differences may affect ACAR function calculated for investigated GaAs and AlAs diamond-like semiconductors.

One can show that over the range of momenta $0 < p < p_F$ the difference between ACAR spectral curves is given, approximately, by the following simple formula:

$$\Delta I(\theta) \approx B - C \times \theta^2, \tag{15}$$

where $B, C \approx const.$ whose magnitudes depend indirectly on the effective charges of As atoms in the investigated materials GaAs and AlAs (see [1] and references therein).

As seen from Fig.7, *a decline* of the difference function of ACAR, calculated by Eq. (15) on the basis of IPM approximation for AlAs and GaAs single crystals, *follows well the experimental data* (compare the data designated by dots and squares in Fig.7, respectively). The magnitude of the difference shown in Fig.7 is small: largest discrepancy in the numeral values calculated for these two materials is observed near to the spectral region adjusted to the Fermi momentum (p_F). Having taken into account a roughness of the approximation used, one may consider an agreement between experimental and calculated data as a good one (the maximal difference between the curves plotted in Fig.7 did not exceed ~ 0,55%).

The *closeness* of this difference of ACAR curves to the one corrected on the basis of the amendments to the electron density around positron caused by the electron-positron Coulomb interaction (see the dot-and-line graphs in Fig.7) deserves special attention: the electron densities obtained by both so-called semiconductor and insulator models [15], respectively, result in the ACAR functions close to the ones obtained both experimentally and by IPM approximation.

Thus, the results of calculations of the electron-positron momentum densities and ACAR curves performed for thin layers of the AlAs-GaAs superlattice as well as for related single crystals of AlAs and GaAs indicate (*i*) smallness of amendments associated with electron-positron Coulomb interactions in the superlattice under study and (*ii*) a necessity of a tangible increase of the sensitivity of the positron particle microprobe when the methods of detection of the electron-positron momentum density distributions are used.

From the viewpoint of a non-destructive/non-contact material characterization this result is quite encouraging because in the case of presence of the defects of a vacancy type in one or another sub-lattices of the superlattice one should expect observing *a marked disturbance* of the electron-positron momentum density distribution which could be detected by determining the properties of the emitted annihilation radiation. In this connection we would like to draw the reader's attention to the Fig.8 where the difference between ACAR spectra obtained for "perfect" single crystals of AlAs and GaAs (shown by squares) is compared with the one obtained in the event that GaAs single crystal

[14] It takes place owing to relatively low efficiency of the electron-positron correlation effects leading to insignificant increase of enhancement factor of the positron annihilation rate in the electron gas of a rather high electron density, equal to ~ 2.0 a.u. [1,8,9]; see also above, Sec.4 and footnotes [12] and [13].

contains the vacancy-type defects (see data designated by dots in Fig.8). In this case the differences between ACAR spectra should be described in terms of the positron trapping and localization in the free volume related to the vacancy whose environment is decorated by the atoms of a certain elemental specificity; these results will be considered elsewhere).

6. Conclusion

The idea of a positron confinement in the perfect lattice of the superlattice GaAs-AlAs has been theoretically analyzed on the basis of the band calculations of the electron-positron momentum density distributions which were performed and then compared with the experimental data obtained *ad hoc* for the constituent parts of GaAs-AlAs superlattice, namely, for GaAs and AlAs single crystals by means of high-precision measurements of the angular correlation of the annihilation radiation (ACAR).

A close proximity of the electron-positron momentum density distributions in AlAs and GaAs crystal lattices, - both in the superlattice under study and the bulk of single crystals, - puts forward a question of a tangible increase of the sensitivity of detecting small (but marked) features of the electron momentum density of the valence band in these chemically related materials.

This problem has been emphasized by comparing ACAR spectral functions obtained for the bulk of AlAs and GaAs single crystals. No significant influence of the electron-positron enhancement factor on the electron-positron momentum density in both calculated and experimental electron-positron momentum distributions has been observed. This fact has been taken into consideration when carrying out the calculation of the electron-positron momentum density distributions in GaAs-AlAs superlattice and related materials.

An effect of confinement of the thermalized positron is predicted for GaAs-AlAs superlattice thus suggesting a preferable presence of positron during its lifetime in the free volume which provides for more favorable energetic conditions. Though this prediction is consistent with the modern conception of the positron partial localization in the field of negative effective charge of As atoms in both AlAs and GaAs “perfect” single crystals, more detailed studies of both phenomena of the positron confinement and its partial localization in the superlattices are required.

As soon as positron-sensitive traps appear in a tangible concentration, - either in the superlattice or in the relevant bulk materials, - the confinement of the delocalized positron changes to a localized state which is characterized, at least, by considerably different electron-positron momentum density distribution which in itself is a fingerprint of a certain microstructure of the positron trap. The appearance of the defects of a vacancy type (e.g., in the crystal lattice of GaAs, - as taken place in the present work) generates the annihilation radiation whose angular correlation indicates directly that in the superlattice under investigation the confinement of positron may change to the positron trapping. We have observed this effect which is crucial for non-dectructive characterization of the heterostructures by means of the positron self-seeking microprobe: this observation gives an opportunity for a direct detecting a signal coming from the vacancy-type defect, i.e. from the free volume associated with the vacancy and its atomic environment; needless to say that the importance of this fact can scarcely be exaggerated.

Acknowledgments

We would like to thank the Condensed Matter Section of the Abdus Salam International Centre for Theoretical Physics, Trieste, Italy, for hospitality and financial assistance that made this work possible. We are also especially indebted to Prof. V.E. Kravtsov for discussions and his interest to these researches.

One of us, N.A., is grateful to German Academic Exchange Service (DAAD) for financial assistance as well as to Prof. R. Krause-Rehberg (the Positron Laboratory at Martin Luther University in Halle) and to Dr. V.V. Emtsev (A.F. Ioffe Physicotechnical Institute, St. Petersburg) for their interest to this work and fruitful discussions.

References

[1] Arutyunov NYu. In*: Condensed matter—new research* (Das, M. P., editor, New York: Nova Science Publishers, 2007) - p. 297.

[2] Nagai, Y., Hasegawa, M., Tang, Z., Hempel, A., Yubuta, K., Shimamura, T., Kawazoe, Y., Kawai, A., and Kano, F., Phys. Rev. B **61**, 6574 (2000).

[3] Dekker, J., Aavikko, R,, Saarinen, K., Appl. Surf. Sci. **194**, 97 (2002).

[4] Sekkal, N., Aurag, H., Superlattices and Microstructures **33**, 63 (2003).

[5] Arutyunov, N.Yu. and Emtsev, V.V., Physica B **401- 402**, 609 (2007).

[6] Cohen, M.L. and. Bergstresser, T.K, Phys. Rev. **141**, 789 (1966).

[7] Aourag, H., Khelifa, B., Belaidi, A., Tadjer, A., Rezki, M., Gamoudi, M., Phys. Stat. Solidi (b) **160**, 193 (1990).

[8] Ferrell, R.A., Rev. Mod. Phys. **28**, 308 (1956).

[9] Barbiellini, B., in: *New Directions in Antimatter Chemistry and Physics* (Surko, C.M. and Gianturco, F.A., editors, printed in Netherlands: Kluwer Academic Publishers, 2001) - p. 127.

[10] Ishibashi, S., Manuel, A.A., Hoffmann, L., and Bechgaard, K., Phys. Rev. B, **55**, 2048 (1997).

[11] Jaros, M., Wong, K.B., Gell, M.A., Phys. Rev. B **31**, 1205 (1985).

[12] Gell, M.A., Ninno, D., Jaros, M., Wolford, D.J., Keuch, T.F., and Bradley, J.A., Phys. Rev. B **35**, 1196 (1987).

[13] Krause-Rehberg R. and Leipner, H.S. *Positron annihilation in semiconductors: Defect studies* **(** Springer-Verlag, Ser. In Solid State Physics, v.127, 1999) – p.378.

[14] Arutyunov, N.Yu., Materials Science Forum **105-110**, 583 (1992).

[15] Puska, M.J. Makinen, S. Manninen, M., Nieminen, R.M., Phys. Rev.B **39**, 7666 (1989).

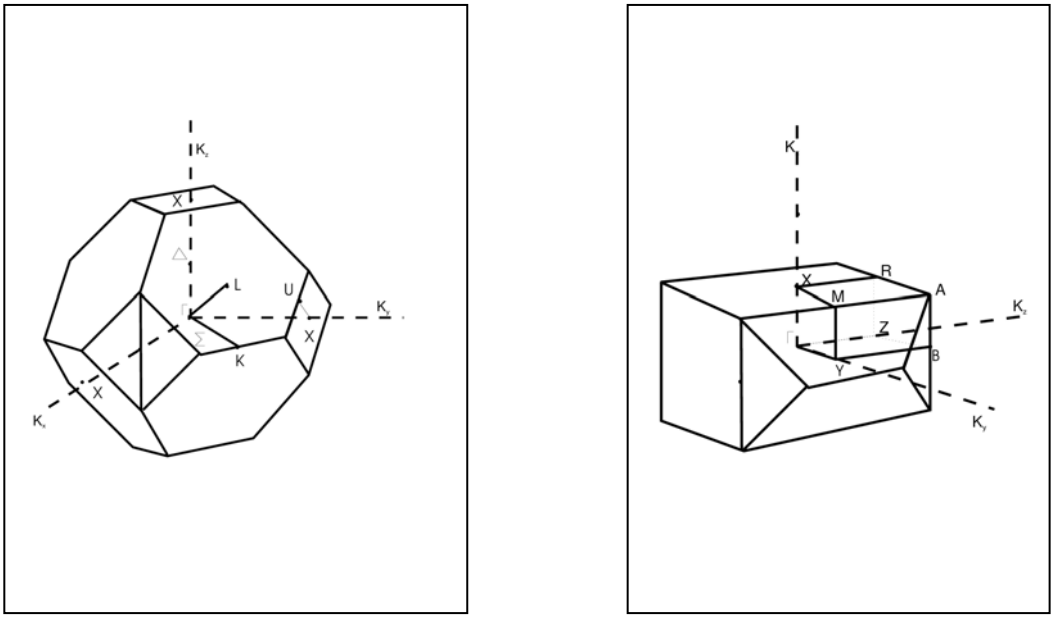

Fig.1. The change of the Brillouin zone in passing from the bulk single crystal AlAs or GaAs, (left), to $(GaAs)_u$-$(AlAs)_v$ superlattice (u, v are the number of layers, see text, Sec.3.2; for more detail see also Fig.1 in Ref. [4]).

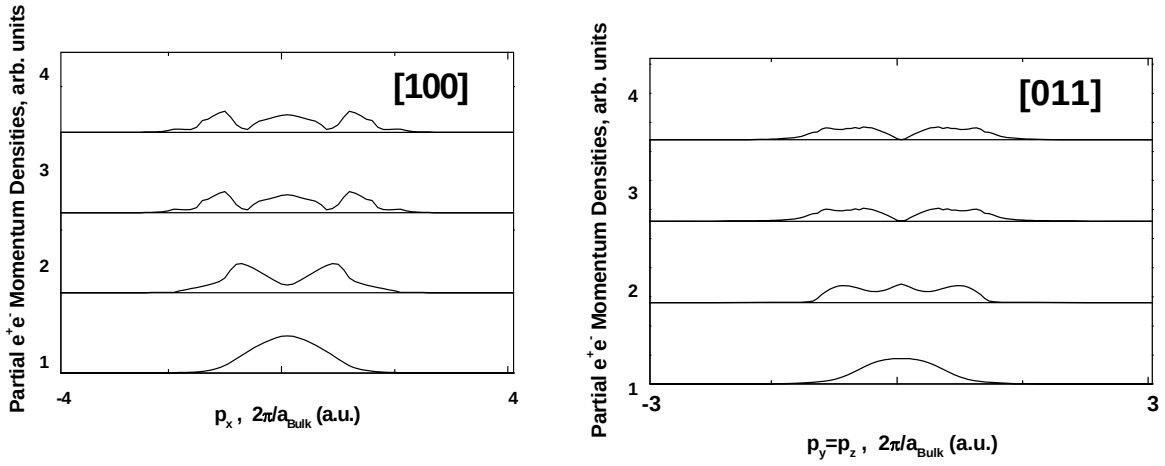

Fig.2. Four partial electron-positron momentum densities in the bulk GaAs single crystal calculated for different crystallographic directions, [100] and [011] (see Sec.3.2 for more detail). The lowest band index corresponds to the electron ground level. For [100] direction $p_y = p_z = 0$ and the only component $p = p_x$ of electron-positron momentum is valid; for [011] crystallographic direction $p_x = 0$ and, accordingly, there is $p = \sqrt{p_y^2 + p_z^2}$.

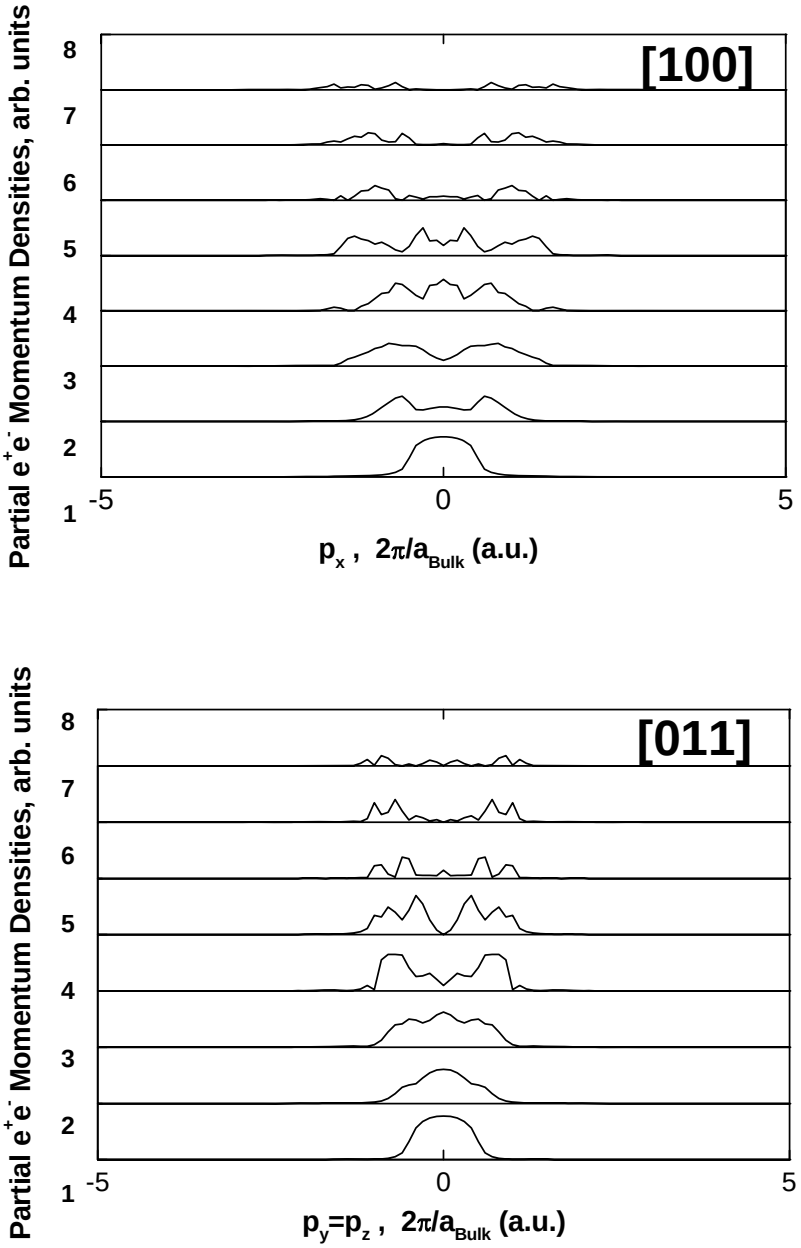

Fig.3. Eight partial electron-positron momentum densities in $(GaAs)_1$-$(AlAs)_1$ superlattice calculated for different crystallographic directions, [100] and [011]. The contribution of 5^{th} partial density is larger than the one of 6^{th} (see Sec.3.2 for more details).

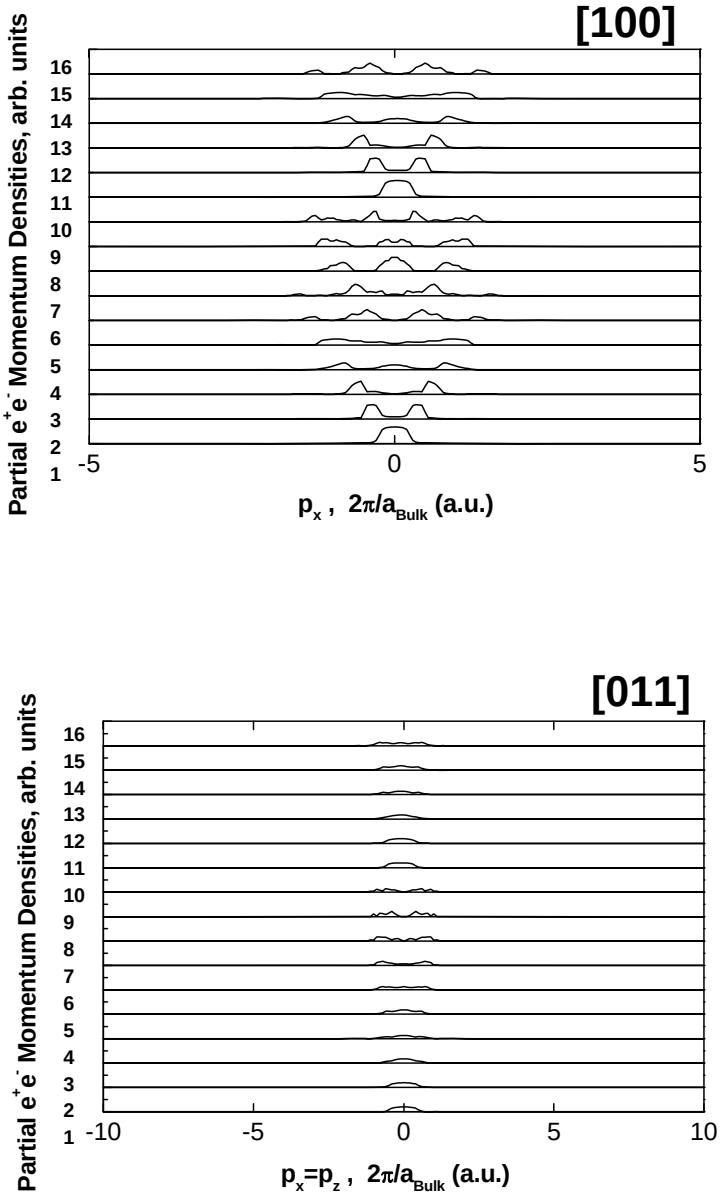

Fig.4. Sixteen partial distributions of the electron-positron momentum densities in $(GaAs)_2$-$(AlAs)_2$ superlattice calculated for different crystallographic directions, [100] and [011]. The contribution of all subbands is comparable (see Sec.3.2 and Sec.3.3 for more details).

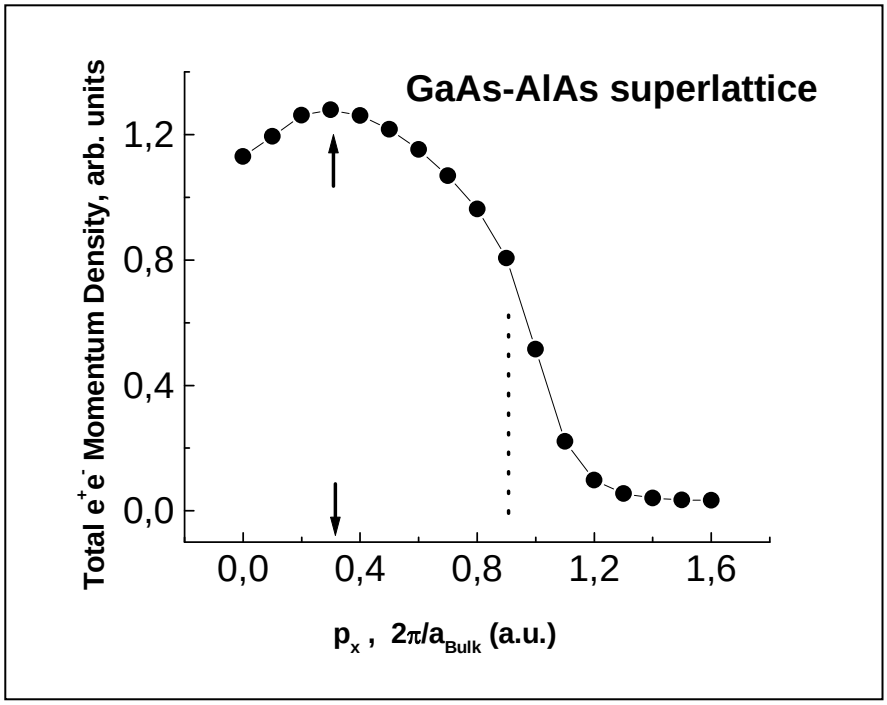

Fig.5. Calculated total electron – positron momentum density distribution for the crystallographic direction [011] in AlAs-GaAs superlattice: arrows and dashed line indicate the position of maximum p_z = 0, 33, *a.u.*, ($p_z \approx 2, 5 \times 10^{-3}\ m_0c$) and the beginning of the interval where the derivative of the distribution is increased, p_z = 0,9 *a.u.* ($\approx 6, 81 \times 10^{-3}\ m_0c$) , respectively.

These features are known to be typical for the electron-positron momentum density distributions registered by ACAR measurements in the diamond-like semiconductors for [110] direction; thus, this observation *directly* indicates reliability and correctness of the whole scheme of calculations described in Sec.3.

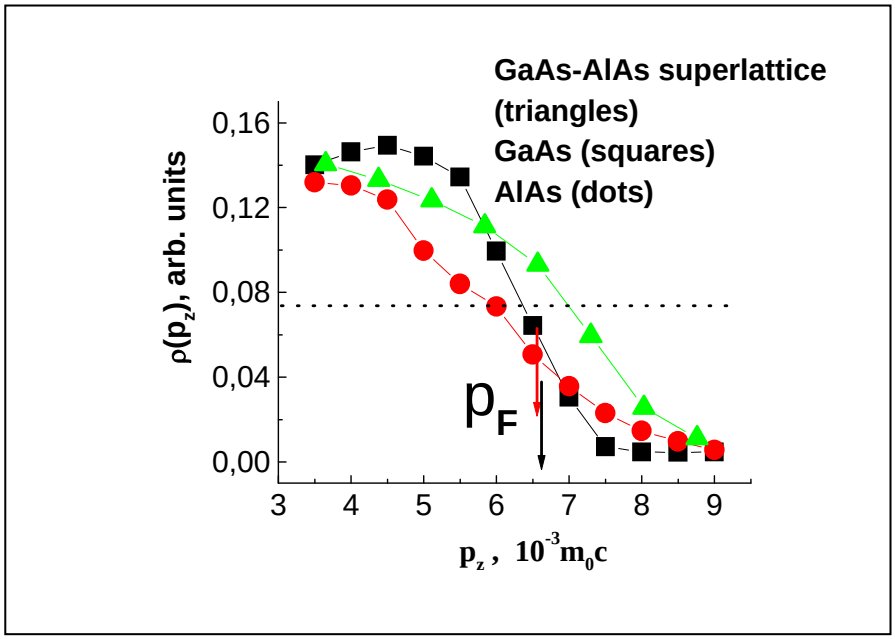

Fig.6. Total electron-positron momentum density distributions $\rho(p_z)$ in the superlattice of GaAs-AlAs calculated for the crystallographic direction [011] (triangles) and the ones reconstructed from ACAR spectra for the constituent materials, AlAs [100] (dots) and GaAs [100] (squares), respectively (see text, Sec.3 and 4).

The range of momenta ~ 3,5 < p_z < p_F is shown to demonstrate *close similarity* of the Fermi distributions of the valence electrons in both GaAs, AlAs single crystals and GaAs-AlAs superlattice under study.

Dashed horizontal line is on the level of HWHM of the distributions whose crosses with the spectral lines indicate the change of the Fermi momentum from ~ 6,25 to ~ 6,95 $\times 10^{-3}$ m_0c in passing from the diamond-like semiconductors (AlAs and GaAs) to the superlattice GaAs-AlAs, respectively.

Upper and lower arrows indicate magnitudes of the Fermi-momenta p_F obtained on the basis of IPM approximation for the valence band of AlAs and GaAs diamond-like semiconductors, respectively; both experimental and calculated p_F magnitudes are very close to each other (see text, Sec.3.3 and Sec.4 for more clarity).

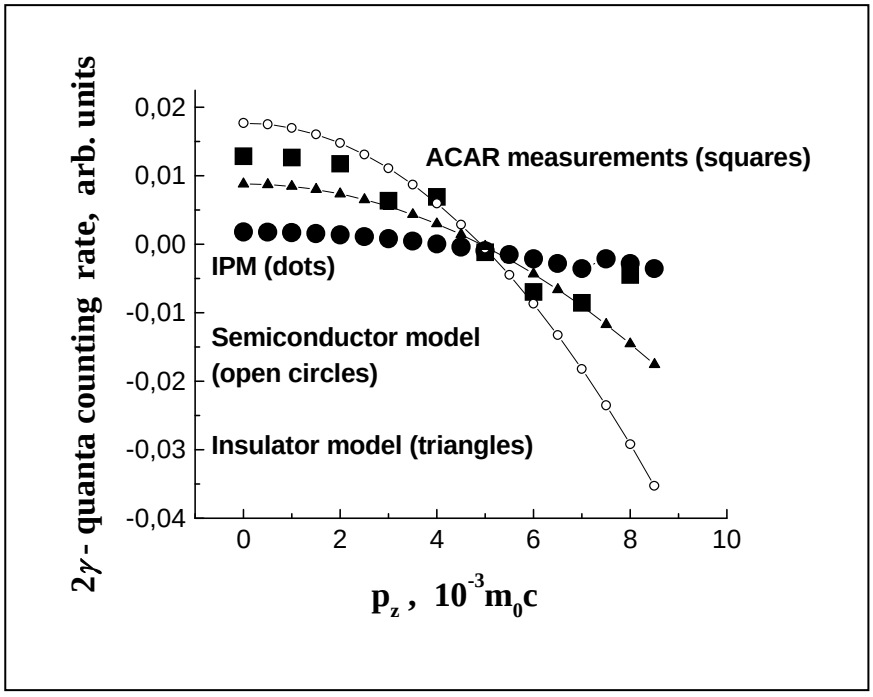

Fig.7. The difference between the ACAR spectral curves for AlAs and GaAs oriented along the crystallographic direction [111]: squares and dots are experimental and calculated data, respectively. The electron-positron interaction has been neglected, so-called independent particle model, IPM, has been used, see e.g. [9] and references therein; see also text and Eq. (15).

The electron-positron Coulomb interaction has been taken into account to calculate the difference between the ACAR spectra plotted by the dot-and-line curves: open circles and triangles designate numeral data obtained by so-called semiconductor and insulator models, respectively. *The insulator and semiconductor models demonstrate similar results.*

Open circles: $r_s^{eff} \approx 2{,}4\, a.u.$ and $r_s^{eff} \approx 2{,}439\, a.u.$ are the magnitudes of the effective electron density calculated for AlAs and GaAs single crystals, respectively; the magnitudes of r_s^{eff} were taken from Table 2 in Ref.[15]).

Triangles: $r_s^{eff} \approx 2{,}35\, a.u.$ and $r_s^{eff} \approx 2{,}4375 a.u.$ values correspond to AlAs and GaAs, respectively, see Table 3, Ref [15]).

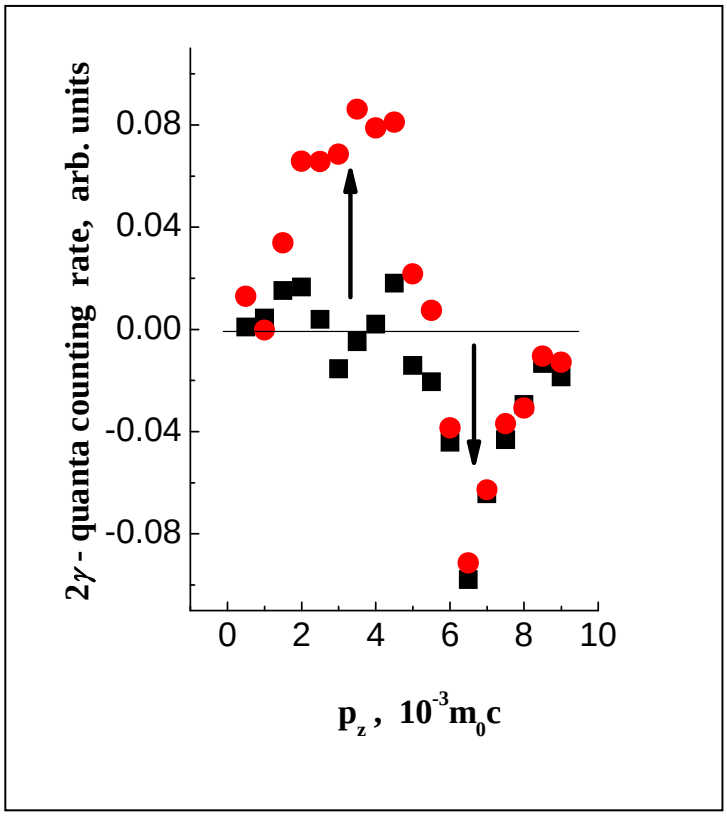

Fig. 8. The difference ACAR curves obtained for AlAs and GaAs single crystals for two cases: 1st – squares: the both crystal lattices of materials are "perfect"; 2nd - dots: AlAs material is "perfect" whereas GaAs crystal lattice contains positron traps which are vacancy-type defects including well-known *EL2* centers (for more details about these traps see, e.g. [13]).

The maximal difference reaches ~ 16% (shown by arrows to guide the eyes); the error does not exceed tripled diameter of dots.